Low-temperature grown wurtzite InxGa1-xN thin films via hollow cathode plasma-assisted atomic layer deposition

7 AUTHORS, INCLUDING:

Eda Goldenberg
Bilkent University
34 PUBLICATIONS   311 CITATIONS

SEE PROFILE

Shahid ALI Leghari
Bilkent University
5 PUBLICATIONS   0 CITATIONS

SEE PROFILE

Ali K. Okyay
Bilkent University
142 PUBLICATIONS   1,172 CITATIONS

SEE PROFILE

Necmi Biyikli
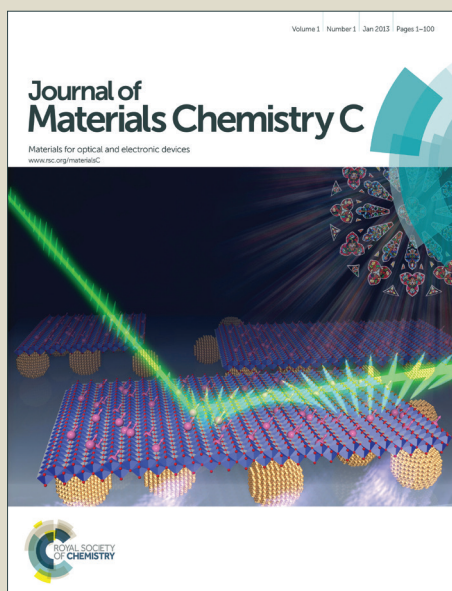Bilkent University
138 PUBLICATIONS   1,150 CITATIONS

SEE PROFILE

Volume 1 | Number 1 | Jan 2013 | Pages 1–100

Journal of
Materials Chemistry C

Materials for optical and electronic devices
www.rsc.org/materialsC

ROYAL SOCIETY
OF CHEMISTRY

This is an *Accepted Manuscript*, which has been through the Royal Society of Chemistry peer review process and has been accepted for publication.

Accepted Manuscripts are published online shortly after acceptance, before technical editing, formatting and proof reading. Using this free service, authors can make their results available to the community, in citable form, before we publish the edited article. We will replace this *Accepted Manuscript* with the edited and formatted *Advance Article* as soon as it is available.

You can find more information about *Accepted Manuscripts* in the **Information for Authors**.

Please note that technical editing may introduce minor changes to the text and/or graphics, which may alter content. The journal's standard **Terms & Conditions** and the **Ethical guidelines** still apply. In no event shall the Royal Society of Chemistry be held responsible for any errors or omissions in this *Accepted Manuscript* or any consequences arising from the use of any information it contains.

ROYAL SOCIETY
OF **CHEMISTRY**

www.rsc.org/materialsC

Journal Name

RSCPublishing

ARTICLE

Low-temperature grown wurtzite In$_x$Ga$_{1-x}$N thin films via hollow cathode plasma-assisted atomic layer deposition

Ali Haider[a,b], Seda Kizir[a,b], Cagla Ozgit-Akgun[a], Eda Goldenberg[a], Shahid Ali Leghari[a,b], Ali Kemal Okyay[a,b,c], Necmi Biyikli[a,b†]

Herein, we report on atomic layer deposition of ternary In$_x$Ga$_{1-x}$N alloys with different indium contents using a remotely integrated hollow cathode plasma source. Depositions were carried out at 200 °C using organometallic Ga and In precursors along with N$_2$/H$_2$ and N$_2$ plasma, respectively. The effect of In content on structural, optical, and morphological properties of In$_x$Ga$_{1-x}$N thin films was investigated. Grazing incidence X-ray diffraction showed that all In$_x$Ga$_{1-x}$N thin films were polycrystalline with hexagonal wurtzite structure. X-ray photoelectron spectroscopy depicted the peaks of In, Ga, and N in bulk of the film and revealed the presence of relatively low impurity contents. In contents of different In$_x$Ga$_{1-x}$N thin films were determined by energy-dispersive X-ray spectroscopy, X-ray photoelectron spectroscopy, and X-ray diffraction. Transmission electron microscopy also confirmed the polycrystalline structure of In$_x$Ga$_{1-x}$N thin films, and elemental mapping further revealed uniform distribution of In and Ga within the bulk of In$_x$Ga$_{1-x}$N films. Higher In concentrations resulted in an increase of refractive indices of ternary alloys from 2.28 to 2.42 at a wavelength of 650 nm. Optical band edge of In$_x$Ga$_{1-x}$N films red-shifted with increasing In content, confirming the tunability of the band edge with alloy composition. Photoluminescence measurements exhibited broad spectral features with an In concentration dependent wavelength shift and atomic force microscopy revealed low surface roughness of In$_x$Ga$_{1-x}$N films with a slight increase proportional to In content.

Introduction

III-nitride semiconductors such as AlN, GaN, InN, and their ternary alloys are highly competitive candidates in the field of optoelectronics.[1–3] Hexagonal wurtzite InN and GaN exhibit direct band gaps of 0.7 and 3.4 eV, respectively. Hence, ternary In$_x$Ga$_{1-x}$N alloys provide band gap values which can be tuned from near ultraviolet to infrared range.[4] In$_x$Ga$_{1-x}$N is a material of prime importance with its applications in In$_x$Ga$_{1-x}$N/GaN based double heterostructure light emitting diodes (LEDs) and potential use in high-efficiency multi-junction thin film solar cells.[5-7] In$_x$Ga$_{1-x}$N alloys are also considered as potential candidates for green LEDs with target wavelength of 525 nm. Green LEDs and deep UV LEDs are conceived as an important challenge in LED technology. Green LEDs with emission wavelength of 525 nm exhibit low efficiency compared to red and blue LEDs and this obstacle is known as the "Green gap".[8]

However, due to the considerable lattice mismatch between GaN and InN, there exists a solid phase miscibility gap in In$_x$Ga$_{1-x}$N alloy system which is a significant hurdle in growing particularly In-rich In$_x$Ga$_{1-x}$N films with decent crystalline quality.[9] Moreover, difference in formation enthalpies and vapor pressures of InN and GaN can lead to either low solubilities or surface segregation of indium in In$_x$Ga$_{1-x}$N alloys.[10,11]

A number of techniques have been utilized for the growth of In$_x$Ga$_{1-x}$N films which include pulsed laser deposition,[12] metal organic chemical vapor deposition (MOCVD),[13] molecular beam epitaxy (MBE),[14] sputtering[15], and hydride vapor phase epitaxy.[16] Among them, MOCVD and MBE are the leading epitaxial growth techniques to grow high quality single-crystalline In$_x$Ga$_{1-x}$N thin films with very low impurity contents. However, both epitaxy methods employ high deposition temperatures, which is a critical limitation in growing indium-rich In$_x$Ga$_{1-x}$N thin films. In addition, growth techniques which require high temperatures pose

incompatibilities with temperature sensitive substrates (*e.g.* glass, flexible polymers). These limitations are the main driving source for a continuous exploration of alternative low temperature processes for the growth of $In_xGa_{1-x}N$ alloys. Furthermore, an alternative growth method in which indium content can be precisely controlled with relative ease for tunable band gap engineering is highly imperative.

Atomic layer deposition (ALD) is a low-temperature vapor phase deposition technique, in which ultra-thin film growth is carried out by repeating two subsequently executed half cycles. ALD offers atomic layer precision in film growth due to self limiting reactions. Unlike conventional CVD, the growth reactor is exposed to a single precursor at a time, separated by purging and/or evacuation periods. When sufficient precursor reactant species are dosed, the surface becomes saturated after occupation of all reactive sites with precursor species. This unique growth mechanism is known as "self-limiting", which refers to a growth regime independent of precursor flux. In addition to sub-monolayer level control over film thickness, self-limiting reactions in ALD facilitate uniform film growth over larger substrates and ultimately conformal growth in deep trenches of high aspect ratio structures provided that dosing and purging times are adjusted optimally.[17–19] Plasma-assisted ALD (PA-ALD) is an energy-enhanced ALD method in which energetic radicals are generated to accelerate the self-terminating ALD reactions. PA-ALD offers several merits over thermal ALD such as improved material properties,[20,21] reduced growth temperatures,[22,23] and increased choice of precursors and materials.[24] Mainly, these superior properties are the result of high reactivity provided by energetic radicals. Moreover, better control of stoichiometry, increased growth rate, minimized/eliminated nucleation delay, and increased process versatility have been reported due to higher degree of freedom in processing conditions (operating pressure, plasma power, plasma exposure time, etc.) of PA-ALD.[24]
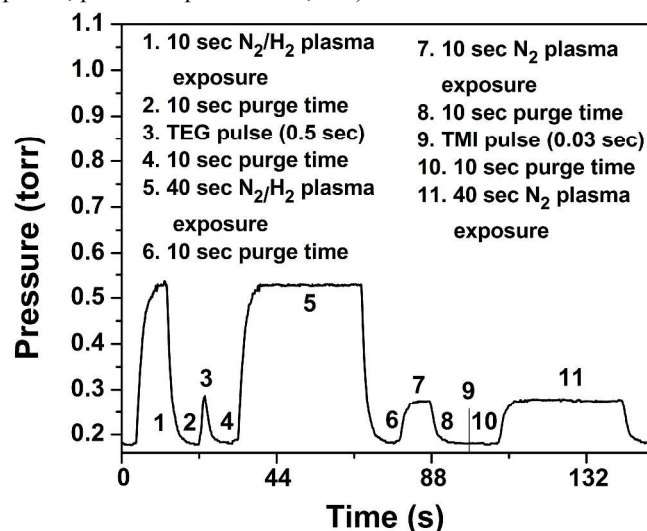

Figure 1. A schematic showing growth process sequence of $In_xGa_{1-x}N$ thin film with single sub cycle of InN and GaN

Alloy thin films can be deposited via PA-ALD either by regulating the vapor pressures of simultaneously exposed precursors or by composing a growth cycle that consists of subcycles of the constituent materials. The latter is termed as "digital alloying" which is a unique and straight forward method of accurately controlling the composition of thin film alloys. In our previous work, we had demonstrated the growth of $Al_xGa_{1-x}N$ thin films via PA-ALD integrated with a hollow cathode plasma source, where we changed the concentration of Al with digital alloying.[21] Recently, Nepal et al.[25] reported plasma assisted atomic layer epitaxy (PA-ALE) of III-nitride ternary thin films using digital alloying method. Here, we report on low-temperature hollow cathode PA-ALD (HCPA-ALD) of crystalline $In_xGa_{1-x}N$ thin films with different indium concentrations and relatively low impurity contents. To the best of our knowledge, this is the first report on self-limiting HCPA-ALD of wurtzite $In_xGa_{1-x}N$ alloys. A detailed material characterization including structural, chemical, morphological, and optical analyzes are presented.

Experimental

Film Deposition

GaN, InN, and $In_xGa_{1-x}N$ thin films were deposited at 200 °C in a modified Fiji F200-LL remote-plasma ALD reactor (Ultratech/CambridgeNanoTech Inc.), which is backed by an adixen ACP 120G dry scroll vacuum pump. Original system was revamped by replacing the quartz-based inductively coupled plasma (ICP) source with stainless steel hollow-cathode plasma (HCP) source (Meaglow Ltd.). The original RF power supply (Seren IPS Inc., R301), matching network controller (Seren IPS Inc., MC2), and automatic matching network (Seren IPS Inc., AT-3) units were used to activate the HCP discharge. Silicon (Si) and double-side polished quartz substrates were cleaned by sequential ultrasonic agitation in 2-propanol, acetone, and methanol, followed by rinsing with DI water and drying with N_2. Native oxide layer on Si was removed by submerging into dilute hydrofluoric acid solution for 2 min, followed by rinsing with DI water and drying with N_2. Substrates were kept at deposition temperature for at least 20 min before the growth process was started. The rotation speed of the Adixen ATH 400 M turbo pump was adjusted in order to keep the reactor pressure fixed at ~150 mTorr during growth sessions, whereas the base pressure of the system was lower than 10^{-5} Torr. Triethylgallium (TEG) and trimethylindium (TMI) were used as gallium and indium metal precursors; whereas N_2/H_2 and N_2 plasma were used as nitrogen precursors for growth of GaN and InN films, respectively. Same nitrogen source was used for respective subcycles of GaN and InN in the main cycle of $In_xGa_{1-x}N$ thin film growth. Organometallic precursors and N_2/H_2 (or N_2) were carried from separate lines using 30 and 100 sccm Ar, respectively. N_2/H_2 (or N_2) gas flow rates and plasma power were constant in all experiments as 50/50 (50) sccm and 300 W, respectively. The system was purged for 10 s after each precursor exposure. Figure 1 shows growth process sequence of $In_xGa_{1-x}N$ thin film. A super

cycle of $In_xGa_{1-x}N$ is depicted which comprise of a single GaN and InN subcycle. Steps 1 to 11 are repeated in sequence to complete one supercycle of $In_xGa_{1-x}N$ thin film. The recipe starts with 10 s N_2/H_2 plasma exposure followed by 10 s purging time. Carrier gas for the precursors and N_2/H_2 plasma is Ar which is also used for purging to remove excess reactant and byproducts. Step 3 is TEG pulse followed by 10 s of purge time. After that, N_2/H_2 plasma is introduced as a second reactant followed by purging. Step 7 is 10 s exposure of N_2 plasma followed by purging. The reactor is then subsequently exposed to TMI pulse followed by 10 s of purge time. TMI pulse is marked by a line and is not visible due to low vapour pressure of TMI. The last two steps are 40 s N_2 plasma exposure and 10 sec of purging time.

Film Characterization

Grazing-incidence X-ray diffraction (GIXRD) and X-ray reflectivity (XRR) measurements were performed in an X'Pert PRO MRD diffractometer (PANalytical) using Cu Kα radiation. GIXRD data was obtained within the 2θ range of 10-90° by the summation of ten scans, which were performed using 0.1° step size and 15 s counting time. Interplanar spacing (d_{hkl}) values were calculated from peak positions using the well-known Bragg's law. Lattice parameters a and/or c were calculated by substituting d_{hkl} values in Eqn. (1), which relates the interplanar spacing (d_{hkl}), miller indices (hkl), and lattice parameters (a and c) for hexagonal crystals.

$$\frac{1}{d^2} = \frac{4}{3}\left(\frac{h^2+hk+k^2}{a^2}\right) + \frac{l^2}{c^2} \qquad (1)$$

Crystallite size values for the GaN, InN, and $In_xGa_{1-x}N$ thin films were estimated from the reflection with maximum intensity using Eqn. (2), the Debye–Scherrer formula:

$$d = \frac{0.9\,\lambda}{B\cos\theta} \qquad (2)$$

Where λ, B, and Θ are the wavelength of the radiation used (Cu Kα = 1.5418 Å), broadening (FWHM), and Bragg diffraction angle of the selected reflection, respectively. The alloy composition x for each $In_xGa_{1-x}N$ film has been calculated using Vegard's law (Eqn. 3), which is a linear relationship between the lattice parameters of an alloy and concentration of constituent elements.

$$a_{In_xGa_{1-x}N} = xa_{InN} + (1-x)a_{GaN} \qquad (3)$$

Elemental composition and chemical bonding states of the $In_xGa_{1-x}N$ thin films were determined by X-ray photoelectron spectroscopy (XPS) using Thermo Scientific K-Alpha spectrometer (Thermo Fisher Scientific) with a monochromatized Al Kα X-ray source. Sputter depth profiling was performed with a beam of Ar ions having an acceleration voltage and spot size of 1 kV and 400 μm, respectively. Surface morphologies of the $In_xGa_{1-x}N$ thin films were revealed using an atomic force microscope (AFM) (PSIA, XE-100E) which was operated in the non-contact mode. Tecnai G2 F30 transmission electron microscope

(TEM) (FEI) was utilized for the high-resolution (HR) imaging of the $In_xGa_{1-x}N$ thin film sample, which was capped with a ~20 nm AlN layer before TEM sample preparation. AlN was deposited at 200 °C using HCPA-ALD, details of which are given elsewhere.[21] TEM sample was prepared by a Nova 600i Nanolab focused ion beam (FIB) system (FEI) with an acceleration voltage of 30 kV using various beam currents ranging from 50 pA to 21 nA. Damage layer was removed by FIB milling at a beam voltage of 5 kV. Elemental mapping was performed in TEM, using an energy dispersive X-ray spectrometer (EDX). Spectral transmission measurements were performed with a UV-VIS spectrophotometer (HR4000CG-UV-NIR, Ocean Optics Inc.) in the wavelength range of 220-1000 nm relative to air, and the optical constants of the films were determined using a variable angle spectroscopic ellipsometer (V-VASE, J.A. Woollam Co. Inc.) which is coupled with rotating analyzer and xenon light source. The ellipsometric spectra were collected at three angles of incidence (65°, 70°, and 75°) to yield adequate sensitivity over the full spectral range. Optical constants and film thickness values were extracted by fitting the spectroscopic ellipsometry data. The numerical iteration was performed to minimize the mean-square error function using WVASE32 software (J.A. Woollam Co. Inc.). The homogeneous Tauc-Lorentz (TL) function was used as an oscillator. The absorption coefficient,

$$\alpha(\lambda) = \frac{4\pi k(\lambda)}{\lambda} \qquad (4)$$

was calculated from the $k(\lambda)$ values determined from the ellipsometry data. Optical band gap (E_g) is expressed by the following equation for direct band gap materials,[26] which can be analytically extracted via extrapolation of the linear part of the absorption spectrum to $(\alpha E)^2 = 0$.

$$\alpha E = A(E - E_g)^{1/2} \qquad (5)$$

$In_xGa_{1-x}N$ film thickness values were theoretically estimated using the following equation.

$$Thickness = n_{GaN(sub)}(Growth\ rate_{GaN})n_{super} + n_{InN(sub)}(Growth\ rate_{InN})n_{super} \quad (6)$$

Where $n_{GaN(sub)}$, $n_{InN(sub)}$, and n_{super} are the number of subcycles of GaN, number of subcycles of InN, and total number of super cycles, respectively. The film thickness values determined from spectroscopic ellipsometry measurements were also cross checked and confirmed by cross-sectional TEM. Photoluminescence (PL) measurements were carried out using a time-resolved fluorescence spectrophotometer (Jobin Yvon, model FL-1057 TCSPC) within the wavelength range of 350– 800 nm.

Results and discussion

$In_xGa_{1-x}N$ layers with different compositions were deposited at 200 °C on pre-cleaned Si (100) and double-side polished quartz substrates. Prior to that, binary GaN and InN thin films

ARTICLE

were deposited with 500-cycle recipes at 200 °C on Si and quartz substrates, which were used as reference/calibration samples inorder to compare their material properties with ternary $In_xGa_{1-x}N$ counterparts. Thicknesses of GaN and InN thin films were measured using a spectroscopic ellipsometer and were found to be 21.5 and 20.0 nm, respectively. These thickness values correspond to growth rates of 0.43 and 0.40 Å/cycle for GaN and InN thin films, respectively. In order to adjust the alloy composition, different numbers of GaN and InN subcycles were used in the main cycle; *i.e.,* GaN:InN = 1:1, 1:3, and 1:5. Ratio of subcycles (RS) was calculated by dividing the number of subcycles of InN to total number of subcycles for GaN and InN; *i.e.,* $n_{s\ InN}/(n_{s\ InN} + n_{s\ GaN})$. The term RS will be used throughout the text to specify different $In_xGa_{1-x}N$ thin films.

Recently, we reported that InN growth using N_2/H_2 plasma as nitrogen source results in a thin film composed of *h*-InN and *t*-InN phases with high percentage of impurities, whereas the film deposited using N_2 plasma is single-phase *h*-InN with low impurity concentrations.[27] Therefore, as mentioned in the experimental section, N_2/H_2 plasma and N_2 plasma were used as nitrogen sources for the growth of GaN and InN films, respectively. Keeping in mind the separate nitrogen precursors used for GaN and InN, 10 s of additional N_2 or N_2/H_2 plasma treatment step (step 1 and 7 in Fig. 1) is used to modify/condition the film surface with suitable plasma species in order to make the substrate compatible for the next InN or GaN subcycle. $In_xGa_{1-x}N$ thin films with RS of 0.5, 0.75, and 0.85 were prepared by the deposition of 500, 300,
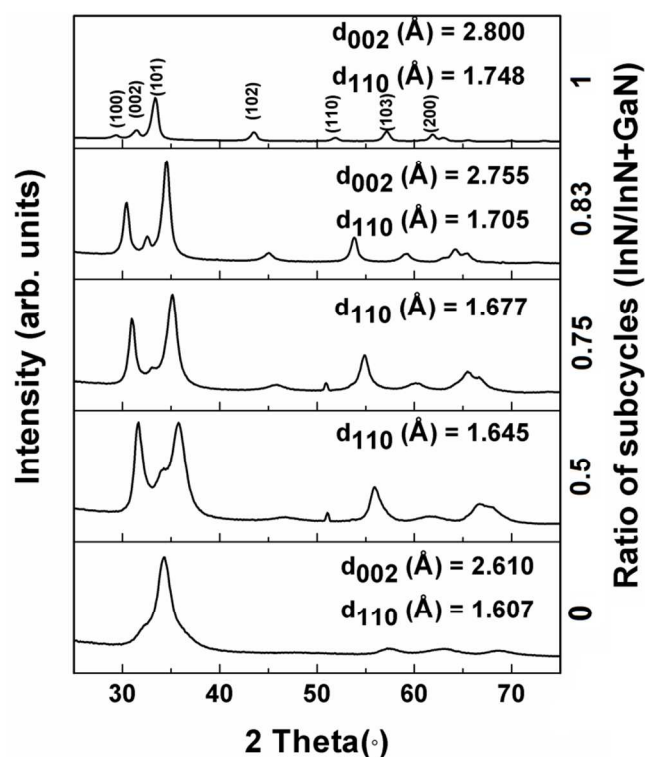
Table 1. Lattice parameters and alloy compositions (as determined by Vegard's law) for GaN, $In_xGa_{1-x}N$, and InN films.

RS[a]	a^b (Å)	c^c (Å)	$x_{Veg}{}^d$
0 (GaN)	3.2071	5.2271	0
0.5	3.2895	-	0.28
0.75	3.3508	-	0.49
0.83	3.4089	5.5130	0.70
1 (InN)	3.4915	5.6106	1

[a]RS is the ratio of subcycles; *i.e.,* $n_{s\ InN}/(n_{s\ InN} + n_{s\ GaN})$. [b]Calculated using the (110) reflection. [c]Calculated using the (002) reflection. [d]x_{Veg} is the alloy composition calculated from *a* values using Vegards's law.

and 200 supercycles, respectively. Thickness values were theoretically estimated using Eqn. 6, and were determined as 41.5, 48.9, and 60.7 nm for $In_xGa_{1-x}N$ thin films having RS of 0.5, 0.75, and 0.83, respectively. Thickness values experimentally measured using spectroscopic ellipsometry were found to be 31.0, 33.0, and 45.0 nm for the same sequence of $In_xGa_{1-x}N$ samples. Deposition rate of GaN on InN and/or deposition rate of InN on GaN might be different than those of GaN on GaN and InN on InN. So, discrepancy between experimental and theoretical thickness values of $In_xGa_{1-x}N$ thin films might be attributed to the resulting uncertainty in GPC values.

GIXRD patterns of GaN, $In_xGa_{1-x}N$, and InN thin films are shown in Fig. 2. GaN and InN thin films were shown to be single-phase as their GIXRD patterns solely exhibited reflections of hexagonal wurtzite GaN (ICDD reference code: 00-050-0792) and hexagonal wurtzite InN (ICDD reference code: 98-015-7515) phases, respectively. The peaks shifted towards lower 2θ values with the increase in InN subcycles. Reflections appeared in the GIXRD patterns of $In_xGa_{1-x}N$ thin films were indexed according to their shift with respect to those of InN and GaN. The shift in peak positions is attributed to In incorporation into wurtzite GaN lattice. The alloy composition *x* for each $In_xGa_{1-x}N$ film has been calculated using Vegard's law (Eqn. 3), which states that there is a linear relationship between the lattice parameters of an alloy and concentration of constituent elements. The interplanar spacing (d_{hkl}) values are indicated in Fig. 2 which were calculated from Bragg's law, using the positions of (002) and/or (110) reflections. Lattice parameters *a* and/or *c* were calculated by substituting the interplanar spacing (d_{hkl}) values in Eqn. 1, which provides a relationship between interplanar spacing (d_{hkl}), miller indices, and lattice parameters for hexagonal crystals.

For $In_xGa_{1-x}N$ thin films having different RS values, *a*-axis lattice parameter was calculated and further substituted in Vegard's law to calculate alloy compositions. Table 1 shows alloy compositions and lattice parameters (*a* and/or *c*)

Figure 2. GIXRD patterns of GaN, InN, and $In_xGa_{1-x}N$ thin films deposited on Si(100) substrates.

for $In_xGa_{1-x}N$ thin films having different RS values. The calculated x values are 0.28, 0.49, and 0.70 for $In_xGa_{1-x}N$ thin films having RS of 0.5, 0.75, and 0.83, respectively. From 2θ positions of (002) and (110) reflections, a and c lattice parameters of GaN and InN were calculated. a and c values are found to be 3.21 and 5.23 Å for GaN, respectively. a and

Table 2. Crystallite size values estimated using Scherrer formula for GaN, $In_xGa_{1-x}N$, and InN films.

RS[a]	(hkl)	K	λ (Å)	FWHM β (°)	θ (°)	t (nm)
0(GaN)	(002)	0.94	1.5418	1.56	17.1	5.5
0.5	(100)	0.94	1.5418	1.16	15.7	7.4
0.75	(100)	0.94	1.5418	0.86	15.4	9.8
0.83	(100)	0.94	1.5418	0.76	15.1	11.3
1(InN)	(100)	0.94	1.5418	1.05	14.8	8.1

[a]RS is the ratio of subcycles; $i.e.,$ $n_{s\ InN}/(n_{s\ InN} + n_{s\ GaN})$.

c values were also determined for InN, which came out as 3.50 and 5.61 Å. The value of a lattice parameters for InN and GaN are in close agreement with the values reported in the literature for strain-free GaN and InN thin films. However, there is a minor variation in c-axis lattice parameters for InN (0.01% lower) and GaN (0.07% higher) layers with respect to the reported values for their nominally strain-free counterparts.[28] The deviation of c lattice parameters from the ideal case indicates that Vegard's law might not be a good-enough approximation in the present case due to presence of strain in the films.

Crystallite sizes (Table 2) were roughly estimated from corresponding dominant reflections using the well-known Debye-Scherrer formula (Eqn. 2), assuming that observed broadening is only due to the size effects thus neglecting instrumental broadening effects.[29] The relatively sharp diffraction peaks obtained from $In_xGa_{1-x}N$ thin films of higher In content suggest that they are composed of larger crystallites. This is evident from decreasing FWHM values of $In_xGa_{1-x}N$ thin films with increase in In concentration. The crystallite size for GaN, $In_xGa_{1-x}N$ (RS=0.5), $In_xGa_{1-x}N$ (RS=0.75), $In_xGa_{1-x}N$ (RS=0.83), and InN were found to be 5.5, 7.4, 9.8, 11.3, and 8.1 nm, respectively.

$In_xGa_{1-x}N$ samples having various In contents were analyzed for elemental compositions, chemical bonding states, and impurity contents of the films using XPS. All spectra have been charge-corrected by referencing the C 1s peak at 284.8 eV. Survey scans from the surface of $In_xGa_{1-x}N$ films indicated the presence of gallium, indium, nitrogen, carbon, and oxygen with Ga 3d, In 3d, N 1s, C 1s, and O 1s peaks, respectively. $In_xGa_{1-x}N$ thin films were etched with Ar^+ ions in order to obtain XPS survey scan from the bulk of the films. Table 3 provides a comparison of the elemental compositions of the $In_xGa_{1-x}N$ films measured from the surface and the bulk. It is apparent that the very surface of all $In_xGa_{1-x}N$ films were contaminated with oxygen (up to 8 at.%) and carbon (up to 23 at.%). XPS elemental quantification analysis

from the bulk of the films revealed no oxygen and carbon in the case of $In_xGa_{1-x}N$ thin film with RS of 0.5. $In_xGa_{1-x}N$ thin films with RS of 0.75 and 0.83 showed low oxygen concentrations of 2.53 and 1.57 at.%, respectively. Only $In_xGa_{1-x}N$ thin film with RS of 0.83 showed bulk carbon contamination of 2.86 at.%, which

Table 3. Elemental composition, Ga/N ratio, and In fractions for$In_xGa_{1-x}N$ films having different RS values.

RS[a]	Elemental composition (at.%)					Ga/N	In fraction[b]
	Ga	In	N	O	C		
0.5 (surface)	28.42	3.78	46.55	8.67	12.58	0.61	0.11
0.5 (bulk)	36.51	2.93	60.56	-	-	0.60	0.07
0.75 (surface)	30.92	6.17	42.46	8.52	11.93	0.72	0.17
0.75 (bulk)	34.83	3.62	59.02	2.53	-	0.59	0.09
0.83 (surface)	31.08	7.48	29.61	8.94	22.90	1.04	0.19
0.83 (bulk)	38.99	6.05	50.83	1.27	2.86	0.76	0.13

[a]RS is the ratio of subcycles;$i.e.,$ $n_{s\ InN}/(n_{s\ InN} + n_{s\ GaN})$. [b]In fraction is obtained using the formula: In (at.%)/ (In (at.%) +Ga(at.%)).

might be due to partially unreacted methyl and ethyl ligands of TMI and TEG, respectively. Those reactive groups might not have reacted sufficiently with the N_2/H_2 or N_2 plasma, and therefore their carbon-containing ligands possibly remained within the growing film. $In_xGa_{1-x}N$ thin films with RS 0.5, 0.75, and 0.83 exhibited Ga/N ratios of 0.60, 0.59, and 0.76 from the bulk of the films, respectively. Although $In_xGa_{1-x}N$ films exhibit higher N at.% as compared to Ga at.% in the bulk of the films, it is worth mentioning that the N at.% is overestimated due to the significant contribution of Ga Auger peak, which overlaps with the N 1s peak.[21,30] In concentrations obtained from the surface for $In_xGa_{1-x}N$ thin films with RS of 0.5, 0.75, and 0.83 are calculated to be 0.11, 0.17, and 0.19, respectively, which are significantly lower than the values obtained using Vegard's law. Possible inhomogeneous distribution of In and Ga atoms in the vicinity of the surface of $In_xGa_{1-x}N$ samples might explain the lower In surface concentration.[30,31] In addition, overestimation of the nitrogen surface contents as explained previously can implicate lowering of In concentration. $In_xGa_{1-x}N$ thin films with RS of 0.5, 0.75, and 0.83 exhibited In concentrations of 0.07, 0.09, and 0.13 from the bulk of the films, respectively. The In content obtained from the bulk of $In_xGa_{1-x}N$ thin films are further reduced in comparison with those obtained from the surface of the films. It indicates the preferential loss of indium with respect to gallium during Ar^+ sputtering, which has been reported in the literature and explained by much lower bond energy of InN (7.7 eV/atom) than GaN (8.9 eV/atom).[32,33]

To clarify the discrepancy in In content of the films obtained via XPS and GIXRD measurements, EDX analysis has been carried out. In concentrations obtained from EDX measurements

ARTICLE

were found as 0.25, 0.33, and 0.64 for $In_xGa_{1-x}N$ films with RS of 0.5, 0.75, and 0.85, respectively. The resulting In concentration

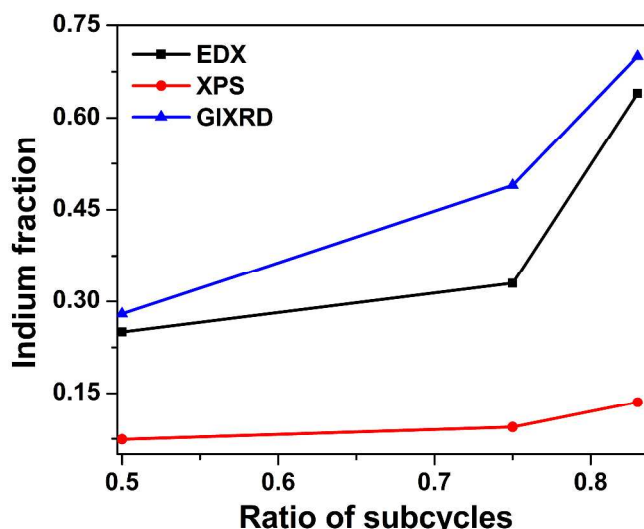**Figure 3.** Indium concentration values obtained from EDX, XPS, and GIXRD for $In_xGa_{1-x}N$ films having different RS values.

values obtained from EDX, XPS, and GIXRD are plotted against RS for $In_xGa_{1-x}N$ films (Fig. 3). EDX analyses reveal closer but still lower In concentration values as compared to the values calculated from Vegard's law. This discrepancy might be attributed to consistent overestimation of Vegard's law assuming the films to be fully relaxed.[34] The difference in In content obtained from XRD and EDX is relatively more reasonable with the downshift in $In_xGa_{1-x}N$ film with RS of 0.75, which can be attributed to the presence of higher strain in $In_xGa_{1-x}N$ film with RS of 0.75.

As a result, EDX appears to be a more appropriate tool for In fraction estimation of $In_xGa_{1-x}N$ thin films due to shortcomings of GIXRD (presence of strain) and XPS (selective etching) for this specific case as explained in detail above. $In_xGa_{1-x}N$ thin films will be specified according to their compositions evaluated from EDX in the following text. In order to check the elemental distribution along the film cross-section, XPS depth profiling was employed on $In_{0.33}Ga_{0.67}N$ sample. Fig. 4 shows the relative atomic concentrations of oxygen, carbon, gallium, indium, and nitrogen through the depth of sample as a function of sputter time. Carbon and oxygen content decreases progressively along the etching direction. Sample was found to be carbon free, while ~2.5 at.% oxygen was found in the bulk of the sample. The results further reveal that $In_{0.33}Ga_{0.67}N$ can be considered homogeneous in terms of elemental (Ga, N, and In) composition within the bulk of the sample.

Chemical bonding states from the bulk of $In_xGa_{1-x}N$ films were studied by the evaluation of their HR-XPS scans and presented in Fig. 5. Different subpeaks used to fit HR-XPS scans were assigned to various chemical states of $In_xGa_{1-x}N$ thin films. Ga 3d HR-XPS (Fig. 5a) scan obtained from the bulk of $In_{0.25}Ga_{0.75}N$ has been deconvoluted into two subpeaks located at 19.82 and 18.67 eV, corresponding to

Ga-N[35–37] and Ga-Ga[35,37] bonds, respectively. Chang et al.[38] reported that Ar^+ etching has led to rearrangement of $In_xGa_{1-x}N$ elemental composition accompanied by presence of metallic Ga. In another study, it has been reported that observed Ga-Ga bond in bulk of the GaN films might form during Ar^+ ion etching owing to the accumulation of metallic Ga on the surface of GaN thin film.[39] In 3d HR-XPS scan (Fig. 5b) obtained from bulk of $In_{0.25}Ga_{0.75}N$ thin film exhibits In-N[40,41] bond by showing doublet of indium 3d core levels which are spin–orbit split to the 3d5/2 peak at 444.5 eV and 3d3/2 peak at 452.1 eV. The N 1s HR-XPS scan (Fig. 5c) obtained from the bulk of $In_{0.25}Ga_{0.75}N$ thin film was fitted using three subpeaks, which were assigned to the N–Ga[35,42] bond (397.0 eV), N-In[40] bond (397.6eV), and Auger Ga[21] peak (395.3 eV). Ga 3d HR-XPS scans (Fig. 5d and 5g) obtained from the bulk of $In_{0.33}Ga_{0.67}N$ and $In_{0.64}Ga_{0.36}N$ thin films followed the trend of Ga 3d HR-XPS scan of $In_{0.25}Ga_{0.75}N$. Both $In_{0.33}Ga_{0.67}N$ and $In_{0.64}Ga_{0.36}N$ thin films manifested two subpeaks for Ga 3d HR-XPS scan, which have been correlated to presence of Ga-N[35–37] (19.5 and 19.3 eV for $In_{0.33}Ga_{0.67}N$ and $In_{0.64}Ga_{0.36}N$, respectively) and Ga-Ga[35,37] bonds (17.5 and 17.7 for $In_{0.33}Ga_{0.67}N$ and $In_{0.64}Ga_{0.36}N$ thin films, respectively). In 3d HR-XPS scans (Fig. 5e and 5h) obtained from bulk of $In_{0.33}Ga_{0.67}N$ and $In_{0.64}Ga_{0.36}N$ thin films followed the footprints of In 3d HR scan of $In_{0.25}Ga_{0.75}N$ thin film, and have been fitted with two peaks each which correspond to In-N[40,41] bond. The N 1s HR-XPS scan (Fig. 5f) obtained from the bulk of $In_{0.33}Ga_{0.67}N$ thin film was identical to N1s HR-XPS spectra of $In_{0.25}Ga_{0.75}N$ thin film. On the other hand, N1s HR-XPS scan (Fig. 5i) obtained from the bulk of $In_{0.64}Ga_{0.36}N$ thin film was fitted using four subpeaks. The first three peaks belong to N–Ga[35,42] bond (397.0 eV), N-In[40] bond (397.7eV), and Auger Ga[21] peaks (395.1 eV), while the additional fourth broad subpeak at 398.3 eV shows the presence of nitrogen sub-oxides[43].

Fig. 6a shows optical transmission spectra of GaN, InN, and $In_xGa_{1-x}N$ thin films deposited on double-side polished

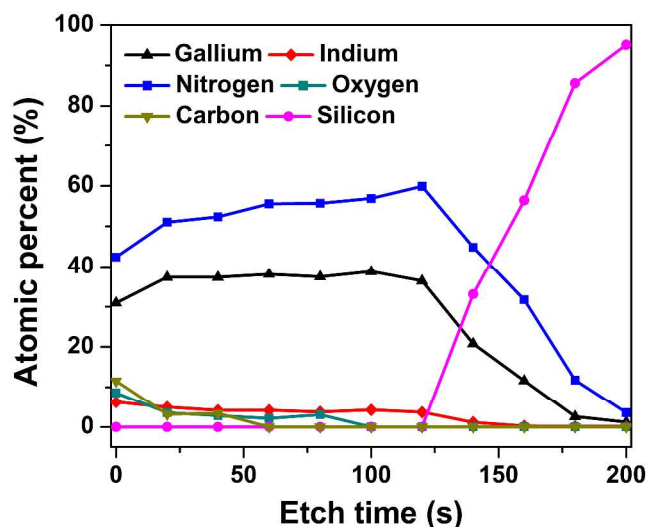**Figure 4.** Compositional depth profile of ~33 nm thick $In_{0.33}Ga_{0.67}N$ thin film deposited on a Si(100) substrate.

quartz wafers. For GaN samples, a significant decrease in the UV transmission was observed at wavelengths <400 nm, which is believed to be caused by the main band-to-band absorption. Transmission values for GaN and $In_xGa_{1-x}N$ thin films were saturated at wavelengths above their transmission band edge. On the other hand, transmission values did not saturate for InN sample, probably due to the high defect density present within the films.[44] InN thin film exhibits 40-50% transmission in the visible regime, which approaches up to 60-70% in the NIR regime. Optical band edge values of the $In_xGa_{1-x}N$ layers shifted towards higher wavelengths with increasing In content as expected, which indicates the tunability of energy band gap by varying In amount.

The optical band gap (E_g) values of $In_xGa_{1-x}N$ films were determined from spectroscopic ellipsometry measurements and related data analysis. The absorption coefficient (α)

values were calculated using Eqn. (4). In Fig. 6b, $(\alpha E)^2$ plots are presented as a function of energy for GaN, InN, and $In_xGa_{1-x}N$ thin films. The fundamental absorption edge in the present thin films is formed by the direct allowed transitions. The optical band gap was determined by extrapolating the linear portion of the plot to $(\alpha E)^2=0$. E_g value of GaN thin film was found to be ~3.45 eV, which is relatively close to the widely accepted value of 3.43 eV for GaN thin films.[45] E_g value of InN was extracted as 1.87 eV. MBE grown epitaxial InN films have shown E_g of 0.7 eV,[46] but earlier accepted values around 1.9 eV are still being reported.[47] There is a significant debate and discrepancy in literature for experimental InN thin film band gap values, which has been ascribed to several reasons such as Burstein-Moss shift, defect levels, and oxygen impurities.[44,48] Optical band gap values of $In_xGa_{1-x}N$ thin films decreased with In content and E_g values were found to be 2.71, 2.45, and 2.18 for $In_{0.25}Ga_{0.75}N$, $In_{0.33}Ga_{0.67}N$, and $In_{0.64}Ga_{0.36}N$ thin films, respectively. A similar dependency of E_g values of $In_xGa_{1-x}N$ thin films on In content has been reported in the literature.[34]

The refractive index dispersion curves of $In_xGa_{1-x}N$ thin films were determined using spectroscopic ellipsometry measurements and the following data analysis. Fig. 7 shows comparison of refractive index values of GaN, InN, and $In_xGa_{1-x}N$ layers deposited on Si (100). The wavelength range for spectroscopic ellipsometry measurements was selected on the basis of optical band edge values of GaN, InN, and $In_xGa_{1-x}N$ samples. Refractive index value of GaN film was measured as 2.10 at 650 nm, which is slightly less than the reported values for polycrystalline GaN thin films.[21] Refractive index value of InN layer was determined as 2.55 at 650 nm, which closely matches with the reported values for polycrystalline InN thin films.[49] As anticipated, refractive index increased from 2.28 to 2.42 as the In fraction of In_xGa_{1-}
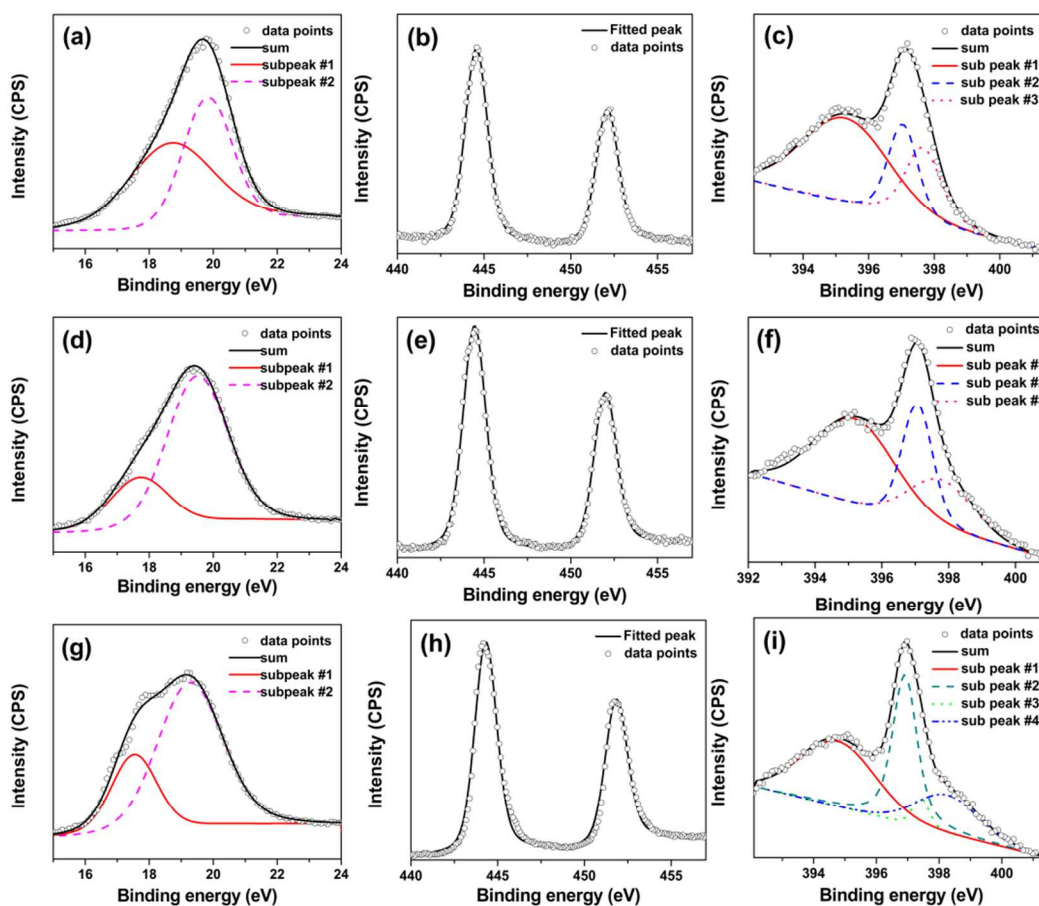
Journal Name

RSC**Publishing**

ARTICLE

Figure 5. Ga 3d, In 3d, and N 1s HR-XPS scans of $In_{0.25}Ga_{0.75}N$ (a, b, c), $In_{0.33}Ga_{0.67}N$ (d, e, f), and $In_{0.64}Ga_{0.36}N$ (g, h, i) thin films deposited on Si(100).

$_x$N samples increased from 0.25 to 0.64. Refractive index of $In_{0.25}Ga_{0.75}N$, $In_{0.33}Ga_{0.67}N$, and $In_{0.64}Ga_{0.36}N$ samples is measured to be 2.28, 2.31, and 2.42, respectively, at 650 nm. The value determined for the $In_{0.64}Ga_{0.36}N$ was found close to that of InN (n = 2.55). The results presented here depict that the refractive index values of $In_xGa_{1-x}N$ thin films change according to alloy composition. XRR measurements revealead mass density of InN, GaN, $In_{0.25}Ga_{0.75}N$, and $In_{0.64}Ga_{0.36}N$ as 5.64, 5.41, 6.23, and 6.57 g/cm^3, respectively. Fitting of XRR data for $In_{0.33}Ga_{0.67}N$ was not good enough to obtain accurate results for that particular film.

TEM experiments were performed on the $In_{0.33}Ga_{0.67}N$ sample. Prior to TEM imaging studies, ~20 nm AlN was deposited on top of $In_{0.33}Ga_{0.67}N$ layer inorder to provide a shelter to protect its crystal structure from a possible damage
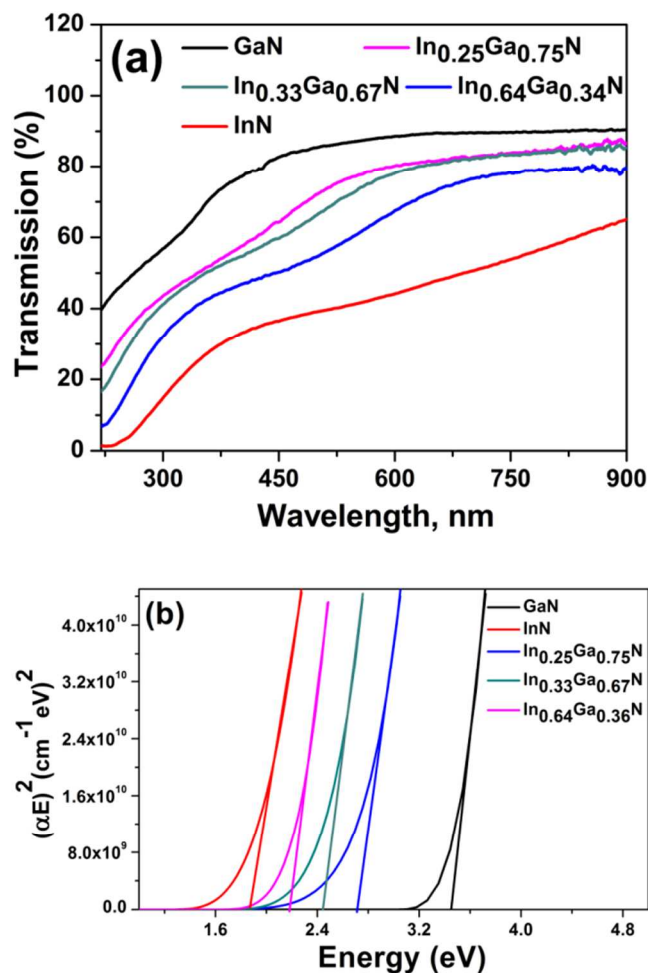
Journal of Materials Chemistry C Accepted Manuscript

Figure 6. (a) Optical transmission spectra of GaN, InN, and $In_xGa_{1-x}N$ thin films deposited on double-side polished quartz substrates. (b) $(\alpha E)^2$ vs. E plots, indicating the optical band gaps of GaN, InN, and $In_xGa_{1-x}N$ thin films.
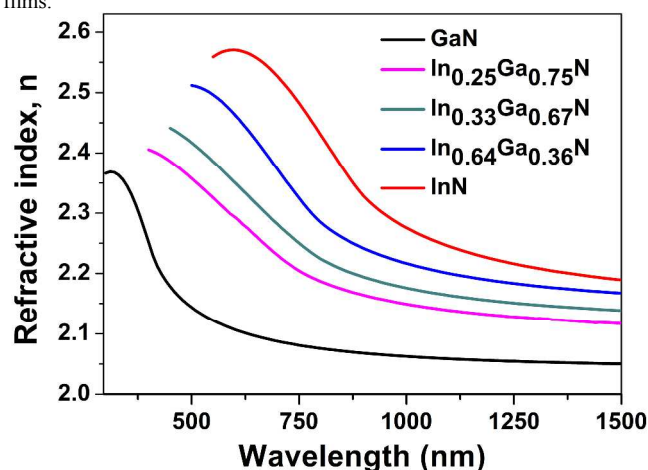

Figure 7. Spectral refractive indices of GaN, InN, and $In_xGa_{1-x}N$ thin films with different Infractions.

of high energy Ga ions of the FIB system, which is used to prepare the samples to be analyzed. Fig. 8a is the cross-sectional TEM image of $In_{0.33}Ga_{0.67}N$ thin film, where one can observe distinct layers of Pt, AlN, $In_{0.33}Ga_{0.67}N$, and Si.

The thickness of $In_{0.33}Ga_{0.67}N$ was measured as ~32 nm from cross-sectional TEM measurements, which is in close agreement with the data obtained from spectroscopic ellipsometry. A ~3 nm thick amorphous SiO_2 layer was observed at the $In_{0.33}Ga_{0.67}N$/Si interface, which is generally named as the "damage layer", formed during the TEM sample preparation using FIB.[50] Fig. 8b shows the HR-TEM image where lattice fringes of $In_{0.33}Ga_{0.67}N$ are organized in different orientations implying the polycrystalline structure of $In_{0.33}Ga_{0.67}N$ film.

Fig. 9 shows EDX elemental maps of Pt, Al, In, Ga, and Si obtained from the AlN-capped $In_{0.33}Ga_{0.67}N$ thin film deposited on Si (100). A cross-sectional portion from specimen was selected and elemental distributions were analyzed by rastering the electron beam point by point over the selected area. The colorized maps show strong contrast among Pt, Al, In, Ga, and Si, and they reveal the elemental distribution along the scanned area.

The characteristic PL emission spectra of $In_{0.25}Ga_{0.75}N$, $In_{0.33}Ga_{0.67}N$, and $In_{0.64}Ga_{0.36}N$ thin films are given in Fig. 10a, b, and c, respectively. The excitation wavelength for GaN and $In_{0.25}Ga_{0.75}N$ thin films was 320 and 450 nm, respectively and it was 550 nm for $In_{0.33}Ga_{0.67}N$ and $In_{0.64}Ga_{0.36}N$ thin films. The GaN spectrum (not shown here) exhibited a broad spectral feature centered at ~360 nm, which results from the main band gap emission in the GaN thin film.[27] However, PL measurement from InN samples did not exhibit considerable emission. In addition to defect bands at lower wavelength, broad spectral features are visible with peaks centered at 508, 618, and 671 nm for $In_{0.25}Ga_{0.75}N$, $In_{0.33}Ga_{0.67}N$, and $In_{0.64}Ga_{0.36}N$ thin films, respectively. These broad spectral features arise from band gap emission of $In_xGa_{1-x}N$ thin films and variation of peak position to higher wavelength indicates the lowering of energy band gap of $In_xGa_{1-x}N$ thin films with increase in In fraction. The broad band emission also points out radiative recombination, which involves structural defects within the films.

Surface morphologies of the $In_xGa_{1-x}N$ thin films were further examined by AFM. Fig.11a, b, and c show the surface scans of $In_{0.25}Ga_{0.75}N$, $In_{0.33}Ga_{0.67}N$, and $In_{0.64}Ga_{0.36}N$ thin films, respectively. All $In_xGa_{1-x}N$ samples revealed island-like granules. Root-mean-square (Rms) surface roughness of the $In_xGa_{1-x}N$ layers showed an increasing trend with In concentration: 0.28, 0.42, and 0.65 nm for $In_{0.25}Ga_{0.75}N$, $In_{0.33}Ga_{0.67}N$, and $In_{0.64}Ga_{0.36}N$ thin films, respectively. Similar trend has also been reported in literature where $In_xGa_{1-x}N$ films grown with plasma-assisted MBE showed increase in surface roughness with In concentration.[51]
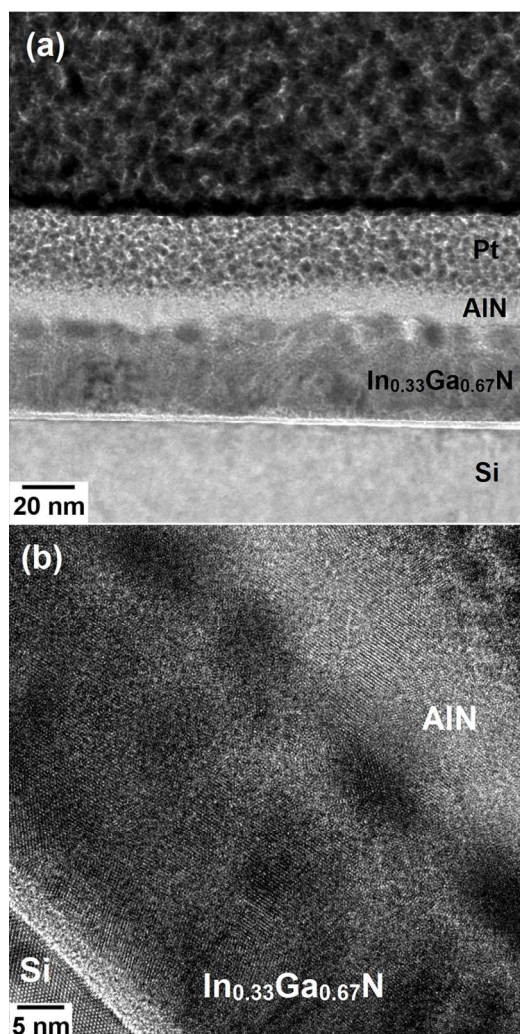
Figure 8. (a) Cross-sectional TEM image of AlN-capped $In_{0.33}Ga_{0.67}N$ thin film deposited on Si(100) substrate. (b) Cross-sectional HR-TEM image of the same sample.

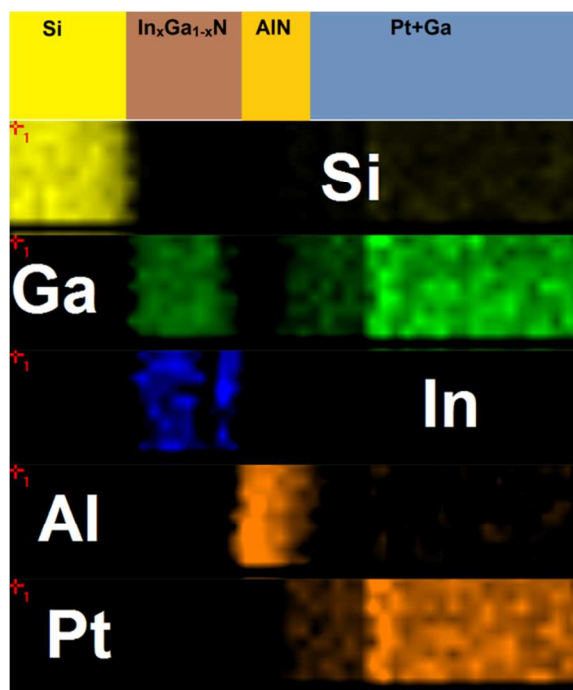**Figure 9.** (a) Elemental map of the AlN-capped $In_{0.33}Ga_{0.67}N$ thin film deposited on Si(100) substrate

Conclusions

$In_xGa_{1-x}N$ thin films have been grown on Si(100) and quartz substrates via HCPA-ALD at 200 °C. Individual GaN and InN subcycles have been tailored in the main ALD growth recipe to change the composition of $In_xGa_{1-x}N$ thin films. Experimental In concentration estimation from EDX analysis turned out to be more accurate as compared to GIXRD and XPS methods due to presence of strain and selective etching of $In_xGa_{1-x}N$ thin films, respectively. In concentration values obtained from EDX analysis were found to be 0.25, 0.33, and 0.64 for $In_xGa_{1-x}N$ films with RS of 0.5, 0.75, and 0.85. $In_xGa_{1-x}N$ films were found to be polycrystalline with hexagonal wurtzite structure as determined by GIXRD and HR-TEM. XPS survey scans from surface and bulk of the films exhibited presence of indium, gallium, and nitrogen along with the presence of relatively low impurity contents. XPS depth profiling revealed homogeneous elemental distribution within the bulk of the sample. Refractive indices of $In_xGa_{1-x}N$ samples increased from 2.28 to 2.42 at 650 nm with increasing In concentration from 0.25 to 0.64. The optical band edge values of $In_xGa_{1-x}N$ thin films decreased with higher In content and band gap values were extracted as 2.71, 2.45, and 2.18 eV for $In_xGa_{1-x}N$ thin films having In concentrations of 0.25, 0.33, and 0.64, respectively. Optical band edge values of the $In_xGa_{1-x}N$ thin films shifted towards higher wavelengths with increasing In content. PL measurements revealed broad spectral features with a wavelength shift depending on In concentration. Root-mean-square (Rms) surface roughnesses of the $In_xGa_{1-x}N$ thin films showed an increasing trend with In content as well. This

Journal Name

ARTICLE

study not only demonstrate the feasibility of low-temperature ternary alloying of crystalline $In_xGa_{1-x}N$ thin films, but the effective tunability of optical and structural properties of $In_xGa_{1-x}N$ as w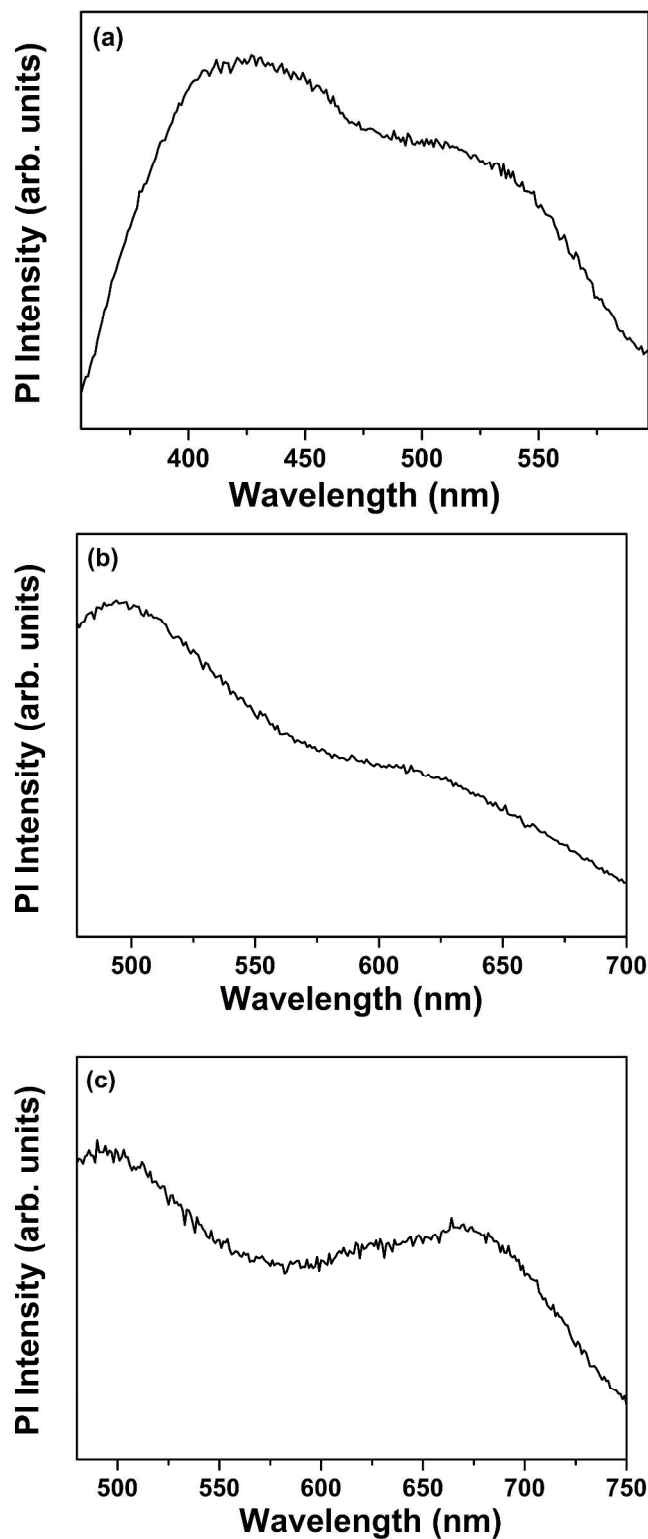ell with compositional digital alloying via PA-ALD technique employing a hollow cathode plasma source. Our initial low-temperature digital alloying results indicate that HCPA-ALD might provide an alternative methodology for the synthesis of In-rich $In_xGa_{1-x}N$ alloys.

Acknowledgements

Figure 10. Room temperature PL spectra of (a) $In_{0.25}Ga_{0.75}N$, (b) $In_{0.33}Ga_{0.67}N$, and (c) $In_{0.64}Ga_{0.36}N$ thin films deposited on Si(100) substrates.
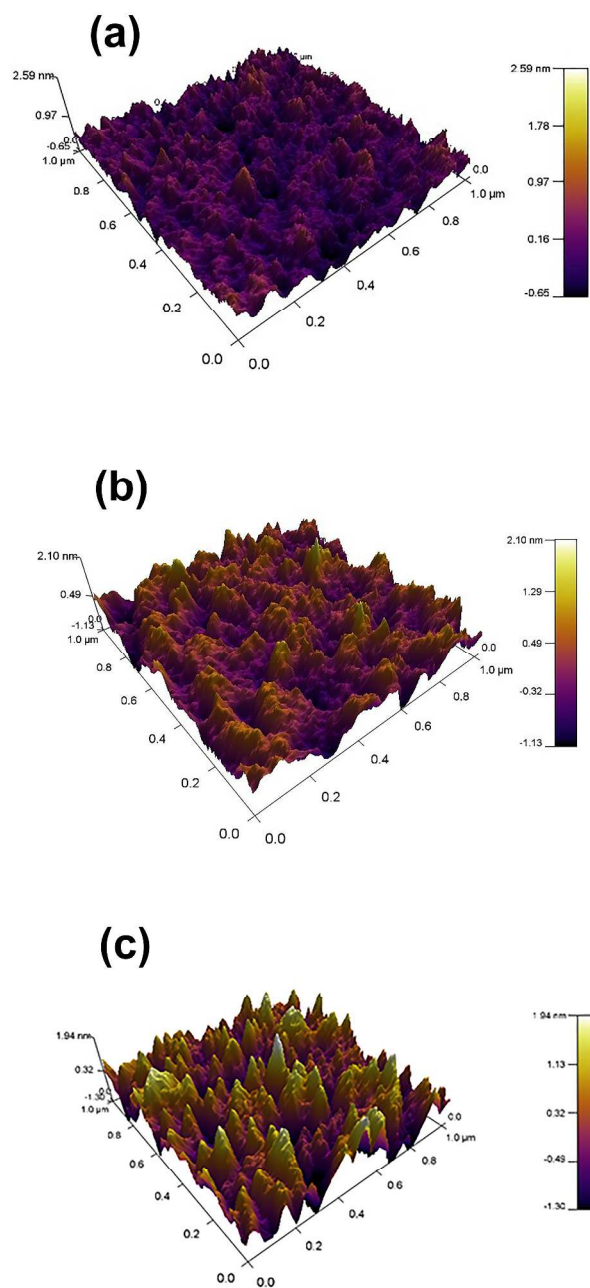
Figure 11. Surface morphologies of (a) $In_{0.25}Ga_{0.75}N$, (b) $In_{0.33}Ga_{0.67}N$, and (c) $In_{0.64}Ga_{0.36}N$ thin films deposited on Si(100) substrates.

Journal of Materials Chemistry C

Page 12 of 14

ARTICLE

View Article Online
DOI: 10.1039/C5TC01733A
Journal Name

Notes and references

[a]UNAM-National Nanotechnology Research Center, Bilkent University, Ankara, 06800, Turkey.
[b]Institute of Materials Science and Nanotechnology, Bilkent University, Ankara, 06800, Turkey.
[c]BilkentUniversity, Department of Electrical and Electronics Engineering, Bilkent, Ankara 06800 Turkey
E-mail: biyikli@unam.bilkent.edu.tr

1 T. Takeuchi, H. Takeuchi, S. Sota, H. Sakai, H. Amano and I. Akasaki, *Japanese J. Appl. Physics,*1997, **36**, 177-179.
2 T. Takeuchi, H. Amano and I. Akasaki, *Japanese J. Appl. Physics*, 2000, **39**, 413–416.
3 F. A. Ponce and D. P. Bour, *Nature*, 1997, **386**, 351–359.
4 J. Wu and W. Walukiewicz, *Superlattices Microstruct.*, 2003, **34**, 63–75.
5 O. Jani, I. Ferguson, C. Honsberg and S. Kurtz, *Appl. Phys. Lett.*, 2007, **91**, 132117.
6 Y. Kuwahara, T. Fujii, T. Sugiyama, D. Iida, Y. Isobe, Y. Fujiyama, Y. Morita, M. Iwaya, T. Takeuchi, S. Kamiyama, I. Akasaki and H. Amano, *Appl. Phys. Express*, 2011, **4**, 4–7.
7 S. Nakamura, M. Senoh and T. Mukai, *Japanese J. Appl. Physics*, 1993, **32**, 8-11.
8 S. J. Chang, W. C. Lai, Y. K. Su, J. F. Chen, C. H. Liu and U. H. Liaw, *IEEE J. Sel. Top. Quantum Electron.*, 2002, **8**, 278–283.
9 G. B. Stringfellow and I. Ho, *Appl. Phys. Lett.*, 1996, **69**, 2701-2703.
10 V. P. Chaly, B. A. Borisov, D. M. Demidov, D. M. Krasovitsky, Y. V. Pogorelsky, A. P. Shkurko, I. A. Sokolov and S. Y. Karpov, *J. Cryst. Growth*, 1999, **206**, 147–149.
11 H. Lu, M. Thothathiri, Z. Wu and I. Bhat, *J. Electron. Mater.*, 1997, **26**, 281–284.
12 A. Kobayashi, J. Ohta and H. Fujioka, *J. Appl. Phys.*, 2006, **99**, 123513.
13 S. Kim, K. Lee, H. Lee, K. Park, C. S. Kim, S. J. Son and K. W. Yi, *J. Cryst. Growth*, 2003, **247**, 55–61.
14 D. N. Nath, E. Gür, S. A. Ringel and S. Rajan, *Appl. Phys. Lett.*, 2010, **97**, 071903.
15 H. Shinoda and N. Mutsukura, *Thin Solid Films*, 2008, **516**, 2837–2842.
16 H.-M. Kim, W. C. Lee, T. W. Kang, K. S. Chung, C. S. Yoon and C. K. Kim, *Chem. Phys. Lett.*, 2003, **380**, 181–184.
17 L. Niinistö, M. Ritala and M. Leskelä, *Mater. Sci. Eng. B*, 1996, **41**, 23–29.
18 S. M. George, *Chem. Rev.*, 2010, **110**, 111–131.
19 M. Leskelä and M. Ritala, *Thin Solid Films*, 2002, **409**, 138–146.
20 A. Haider, C. Ozgit-Akgun, E. Goldenberg, A. K. Okyay and N. Biyikli, *J. Am.Ceram. Soc.*, 2014, **12**, 4052-4059.
21 C. Ozgit-Akgun, E. Goldenberg, A. K. Okyay and N. Biyikli, *J. Mater. Chem. C*, 2014, **2**, 2123-2136.
22 S. E. Potts, W. Keuning, E. Langereis, G. Dingemans, M. C. M. van de Sanden and W. M. M. Kessels, *J. Electrochem. Soc.*, 2010, **157**, 66-74.
23 M. Caymax, G. Brammertz, A. Delabie, S. Sioncke, D. Lin, M. Scarrozza, G. Pourtois, W. -E. Wang, M. Meuris and M. Heyns, *Microelectron. Eng.*, 2009, **86**, 1529–1535.
24 H. B. Profijt, S. E. Potts, M. C. M. van de Sanden and W. M. M. Kessels, *J. Vac. Sci. Technol. A Vacuum, Surfaces, Film.*, 2011, **29**, 050801.
25 N. Nepal, V. R. Anderson, J. K. Hite and C. R. Eddy, *Thin Solid Films*, 2015, **589**, 47-51.
26 E. Rosencher, Optoelectronics, 2002, 304.
27 C. Ozgit-Akgun, E. Goldenberg, S. Bolat, B. Tekcan, F. Kayaci, T. Uyar, A. K. Okyay and N. Biyikli, *Phys. Status Solidi*, 2015, **12**, 394-398.
28 M. A. Moram and M. E. Vickers, *Reports Prog. Phys.*, 2009, **72**, 036502.
29 B. D. Cullity, *Elemets X-ray Diffr.*, 1956, 431–453.
30 M. Krawczyk, W. Lisowski, J. W. Sobczak, A. Kosiński, A. Jablonski, C. Skierbiszewski, M. Siekacz and S. Wiązkowska, *J. Alloys Compd.*, 2011, **509**, 9565–9571.
31 H. Chen, R. Feenstra, J. Northrup, T. Zywietz and J. Neugebauer, *Phys. Rev. Lett.*, 2000, **85**, 1902–1905.
32 J. Northrup and J. Neugebauer, *Phys. Rev. B*, 1999, **60**, R8473–R8476.
33 J. E. Northrup, L. T. Romano and J. Neugebauer, *Appl. Phys. Lett.*, 1999, **74**, 2319-2321.
34 S. R. Meher, a. Subrahmanyam and M. K. Jain, *J. Mater. Sci.*, 2013, **48**, 1196–1204.
35 M. Kumar, A. Kumar, S. B. Thapa, S. Christiansen and R. Singh, *Mater. Sci. Eng. B Solid-State Mater. Adv. Technol.*, 2014, **186**, 89–93.
36 P. Kumar, M. Kumar, Govind, B. R. Mehta and S. M. Shivaprasad, *Appl. Surf. Sci.*, 2009, **256**, 517–520.
37 H. Xiao, R. Liu, H. Ma, Z. Lin, J. Ma, F. Zong and L. Mei, *J. Alloys Compd.*, 2008, **465**, 340–343.
38 C.-A. Chang, C.-F. Shih, N.-C. Chen, T. Y. Lin and K.-S. Liu, *Appl. Phys. Lett.*, 2004, **85**, 6131-6133.
39 K. S. A. Butcher, Afifuddin, T. L. Tansley, N. Brack, P. J. Pigram, H. Timmers, K. E. Prince and R. G. Elliman, *Appl. Surf. Sci.*, 2004, **230**, 18–23.
40 H. Parala, A. Devi, F. Hipler, E. Maile, A. Birkner, H. W. Becker and R. A. Fischer, *J. Cryst. Growth*, 2001, **231**, 68–74.
41 Y. Huang, H. Wang, Q. Sun, J. Chen, J. F. Wang, Y. T. Wang and H. Yang, *J. Cryst. Growth*, 2005, **281**, 310–317.
42 Z. Majlinger, A. Bozanic, M. Petravic, K. J. Kim, B. Kim and Y. W. Yang, *Vacuum*, 2009, **84**, 41–44.
43 H. Shinoda and N. Mutsukura, *Diam. Relat. Mater.*, 2002, **11**, 896–900.
44 K. S. A. Butcher and T. L. Tansley, *Superlattices Microstruct.*, 2005, **38**, 1–37.
45 M. M. El-Nahass and A. A. M. Farag, *Opt. Laser Technol.*, 2012, **44**, 497–503.
46 V. Y. Davydov, a. a. Klochikhin, R. P. Seisyan, V. V. Emtsev, S. V. Ivanov, F. Bechstedt, J. Furthmüller, H. Harima, a. V. Mudryi, J. Aderhold, O. Semchinova and J. Graul, *Phys. Status Solidi Basic Res.*, 2002, **229**, 1972–1974.
47 A. K. Mann, D. Varandani, B. R. Mehta and L. K. Malhotra, *J. Appl. Phys.*, 2007, **101**, 084304.
48 T. L. Tansley and C. P. Foley, *J. Appl. Phys.*, 1986, **59**, 3241–3244.
49 L. F. Jiang, W. Z. Shen, H. F. Yang, H. Ogawa and Q. X. Guo, *Appl. Phys. A Mater. Sci. Process.*, 2004, **78**, 89–93.

50   J. Mayer, L. a Giannuzzi, T. Kamino and J. Michael, *MRS Bull.*,
     2007, **32**, 400–407.

51   E. J. Shin, S. H. Lim, M. Jeong, D. S. Lim, S. K. Han, H. S. Lee, S.
     K. Hong, J. Y. Lee and T. Yao, *Thin Solid Films*, 2013, **546**, 42–47.

Journal of Materials Chemistry C Accepted Manuscript
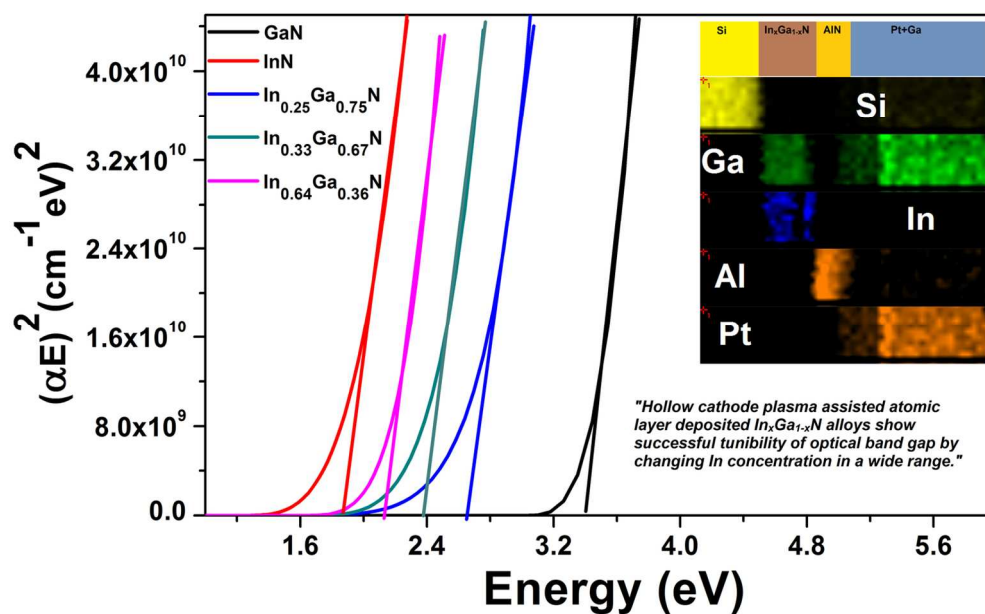
Hollow cathode plasma assisted atomic layer deposited $In_xGa_{1-x}N$ alloys show successful tunibility of optical band gap by changing In concentration in a wide range

133x83mm (300 x 300 DPI)